

ExplainerPFN: Towards tabular foundation models for model-free zero-shot feature importance estimations

Joao Fonseca^{1,2} Julia Stoyanovich²

Abstract

Computing the importance of features in supervised classification tasks is critical for model interpretability. Shapley values are a widely used approach for explaining model predictions, but require direct access to the underlying model, an assumption frequently violated in real-world deployments. Further, even when model access is possible, their exact computation may be prohibitively expensive. We investigate whether meaningful Shapley value estimations can be obtained in a *zero-shot* setting, using only the input data distribution and no evaluations of the target model. To this end, we introduce ExplainerPFN, a tabular foundation model built on TabPFN that is pretrained on synthetic datasets generated from random structural causal models and supervised using exact or near-exact Shapley values. Once trained, ExplainerPFN predicts feature attributions for unseen tabular datasets without model access, gradients, or example explanations.

Our contributions are fourfold: (1) we show that few-shot learning-based explanations can achieve high fidelity to SHAP values with as few as two reference observations; (2) we propose ExplainerPFN, the first zero-shot method for estimating Shapley values without access to the underlying model or reference explanations; (3) we provide an open-source implementation of ExplainerPFN, including the full training pipeline and synthetic data generator; and (4) through extensive experiments on real and synthetic datasets, we show that ExplainerPFN achieves performance competitive with few-shot surrogate explainers that rely on 2–10 SHAP examples¹.

¹INESC-ID, Lisbon, Portugal ²New York University, New York, USA. Correspondence to: Joao Fonseca <joaofonseca@nyu.edu>.

Preprint. February 2, 2026.

¹We make all the code developed for this project available at <https://github.com/joaofonseca/ExplainerPFN>

1. Introduction

In many real-world applications, machine learning (ML) systems make or assist in making high-stakes decisions, such as loan approvals, hiring, or medical diagnoses. These models are often proprietary and operate as black boxes, leaving users and regulators without insight into how decisions are made. Consider an individual who is denied a loan by a proprietary, black-box ML system. The applicant may reasonably ask which factors contributed most to the decision. Alternatively, stakeholders may wish to ensure that the model does not distinguish based on protected attributes like race or gender. However, access to the underlying model is rarely granted, and feature-level explanations are almost never provided. In such settings, the ability to estimate feature attributions *without* model access becomes crucial for auditing decisions, identifying potential biases, and improving transparency.

This challenge reflects a broader trend in modern ML. Many real-world models operate behind closed APIs for reasons of privacy, intellectual property, or security, limiting direct model access. At the same time, tabular data has received comparatively little attention in foundation model research. Recent work highlights both the need for methods that can analyze data without direct access to sensitive models (Hod et al., 2025) and the potential of large tabular models to transfer knowledge across heterogeneous tabular tasks (Van Breugel & Van Der Schaar, 2024).

Recent studies raise questions about the stability and interpretability of existing feature attribution methods. While covariate-based importance measures are statistically well motivated in many settings (Verdinelli & Wasserman, 2024), Shapley-based explanations can be sensitive to correlations among input features, and even simple changes in data representation can substantially alter SHAP-based attributions (Hwang et al., 2025). Rather than being a purely methodological limitation, these sensitivities suggest that the data distribution itself plays a central role in shaping feature attributions. This observation motivates the possibility of learning attribution patterns directly from data, without requiring access to the underlying model.

Contributions. We study zero-shot estimation of Shapley

value feature attributions using only the input data distribution and model predictions. We approach this problem through tabular foundation models and in-context learning, and ask whether Shapley values can be estimated in highly resource-constrained settings without access to the model, gradients, or reference SHAP explanations. We introduce ExplainerPFN, a tabular foundation model built on top of TabPFN (Hollmann et al., 2023) that predicts Shapley values in a fully zero-shot manner. Our main contributions are:

- 1 We show that few-shot learning-based explanations can achieve high fidelity to true SHAP values, in some cases with as few as 2 reference observations.
- 2 We propose the first *zero-shot* method for estimating Shapley values, requiring no access to the underlying ML model or feature attribution examples.
- 3 We provide an open-source implementation of ExplainerPFN, including the training pipeline, pretrained weights, and a synthetic data generator for tabular foundation model pretraining, adapted from the TabPFN synthetic prior-fitting procedure and redesigned for feature attribution learning.
- 4 Through extensive experiments on real and synthetic datasets, we demonstrate that ExplainerPFN achieves performance competitive with few-shot surrogate explainers requiring 2–10 SHAP examples from the target model.

Overall, our results suggest that meaningful feature attribution patterns can be recovered *directly* from the data distribution, opening a new direction in zero-shot explainability using tabular foundation models.

2. Preliminaries and Background

Shapley values. The Shapley value is a concept from cooperative game theory that provides a fair way to distribute the total gains (or costs) among the players based on their individual contributions to the overall outcome (Shapley, 1953). It has been widely adopted in explainable AI (xAI) to attribute feature importance in ML models.

Let $f: \mathbb{R}^m \rightarrow \mathbb{R}$ be a predictive model, $x_i = (x_i^1, \dots, x_i^m)$ an input instance², and $M = \{1, \dots, m\}$ the set of feature indices. Given a dataset $X = \{x_1, \dots, x_n\}$, where x_i^j denotes the value of the j -th feature for instance i , the Shapley value ϕ_i^j is computed as follows:

$$\Delta_j(S) := \mathbb{E} [f(x_i) | x_i^{S \cup \{j\}}] - \mathbb{E} [f(x_i) | x_i^S] \quad (1)$$

$$w(S) := \frac{|S|!(m - |S| - 1)!}{m!} \quad (2)$$

$$\phi_i^j := \sum_{S \subseteq M \setminus \{j\}} w(S) \Delta_j(S) \quad (3)$$

²We use “input instance” and “observation” interchangeably.

where S is a subset of features not including feature j , $\mathbb{E} [f(x_i) | x_i^S]$ is the expected model output conditioned on the feature values in S , and $|S|$ is the cardinality of S . Intuitively, $\Delta_j(S)$ represents the marginal contribution of feature j , which is weighted by $w(S)$ to account for all feature coalitions. Finally, ϕ_i^j is obtained by summing the weighted marginal contributions over all subsets S .

SHAP. SHapley Additive exPlanations (SHAP) (Lundberg & Lee, 2017) is a popular game-theoretic framework for local explanations of ML model predictions in the form of feature importance scores derived from Shapley values. For general models (including neural networks), the exact computation of SHAP scores is intractable ($\#P$ -hard) (Arenas et al., 2023). Consequently, SHAP (and other Shapley value-based frameworks) typically approximate feature importance either via Monte Carlo sampling over S , by limiting the maximum coalition size (Pliatsika et al., 2025), or via model-specific approximations such as TreeSHAP (Lundberg et al., 2020). These strategies introduce a trade-off between computational cost and fidelity of the explanation, defined by how well the resulting feature importance scores reconstruct the model output. Recent works aim to improve the computational efficiency of SHAP computation in particular settings (Mitchell et al., 2022; Arenas et al., 2023), typically in polynomial time. Importantly, these methods still require access to the underlying model f . Instead, we consider the problem of estimating feature importance when f is not directly accessible. We assume access to X and the corresponding model predictions $\hat{Y} := \hat{y}_1, \dots, \hat{y}_n$, where $\hat{y}_i := f(x_i)$, and our objective is to approximate ϕ_i^j .

Tabular foundation models (TFM). Formally, a TFM is a pretrained mapping $F: \mathcal{X} \times \mathcal{D} \rightarrow \mathbb{R}$, where $\mathcal{X} \subseteq \mathbb{R}^m$ denotes the feature space and \mathcal{D} denotes the space of possible context datasets, respectively. At inference time, predictions for x_i are obtained by conditioning on a context dataset $D = \{(x_1, y_1), \dots, (x_n, y_n)\} \subseteq \mathcal{D}$, i.e., $\hat{y}_i := F(x_i | D)$. Thus, TFM leverage in-context learning (Brown et al., 2020), where F is defined based on priors learned during pretraining (e.g., via synthetic prior-fitting (Hollmann et al., 2023) or SSL (Ma et al., 2025)) to make predictions based on D , without gradient-based adaptation.

3. Problem Formulation

Problem statement. We study the problem of estimating per-instance feature importance for a fixed but inaccessible predictive model $f^b: \mathcal{X} \rightarrow \mathbb{R}$, instantiated from the general predictive model f defined in Section 2. Given a dataset of inputs $X = \{x_1, \dots, x_n\} \subset \mathcal{X}$ and the corresponding model predictions $\hat{Y} = \{\hat{y}_1, \dots, \hat{y}_n\}$, where $\hat{y}_i = f^b(x_i)$, our goal is to estimate, for each instance x_i , a feature importance vector $\phi_i = (\phi_i^1, \dots, \phi_i^m) \in \mathbb{R}^m$ that approximates the Shapley values of the underlying model.

We consider problem settings that differ in the degree of access to the model f^b and to reference feature importance scores, ranging from few-shot to fully zero-shot regimes.

Few-shot feature importance estimation. Let f^b be a base model trained over a distinct labeled dataset D_{base} . Given a small set of instances $X_{\text{train}} \subset \mathcal{X}$ and their corresponding model predictions $\hat{Y}_{\text{train}} = \{f^b(x) \mid x \in X_{\text{train}}\}$ (ground-truth labels are not required), we assume access to a limited collection of reference feature importance vectors $\Phi_{\text{train}} = \{\phi_i \mid x_i \in X_{\text{train}}\}$.

This setting captures two common scenarios: (1) access to f^b is limited, for example via a rate-limited API, so only a small number of reference feature importance vectors can be computed directly, or (2) f^b is entirely inaccessible, but Φ_{train} has been precomputed. In either case, the objective is to learn a surrogate model g such that, for an unseen instance $x_i \in X_{\text{test}}$ with predicted output $\hat{y}_i = f^b(x_i)$, the surrogate produces an estimate $g(x_i, \hat{y}_i) \approx \phi_i^{\text{test}}$.

In this work, we use a tabular foundation model as the surrogate, performing in-context learning over the few-shot reference set. While our primary contribution targets the zero-shot setting, described next, we revisit the few-shot formulation in Section 5 for benchmarking against surrogate explainers with limited reference explanations.

Zero-shot feature importance estimation. Let f^b be a fixed but inaccessible predictive model and suppose that no reference feature importance vectors are available, i.e., $\Phi_{\text{train}} = \emptyset$. Given an unseen dataset $X_{\text{test}} \subset \mathcal{X}$ and the corresponding model predictions $\hat{Y}_{\text{test}} = \{\hat{y}_i \mid x_i \in X_{\text{test}}\}$, the objective is to estimate the feature importance vectors $\Phi_{\text{test}} = \{\phi_i^{\text{test}} \mid x_i \in X_{\text{test}}\}$ without querying f^b and without access to any precomputed explanations.

In this setting, a zero-shot explainer must approximate the mapping $(x_i, \hat{y}_i) \mapsto \phi_i^{\text{test}}$ without observing any triplets (x_i, \hat{y}_i, ϕ_i) either at training time or at inference time. The only information available at inference time is the pair $(X_{\text{test}}, \hat{Y}_{\text{test}})$. In Section 4 we describe how tabular foundation models can be adapted to address this setting.

4. ExplainerPFN

ExplainerPFN addresses the zero-shot feature importance estimation problem of Section 3. It adapts the TabPFN framework (Hollmann et al., 2023) but replaces its predictive objective with a Shapley-value meta-learning objective. ExplainerPFN is trained on a large meta-distribution of synthetic tabular tasks to learn a mapping from input-prediction pairs to per-instance feature attributions, without ever observing real-world explanations. At inference time, ExplainerPFN acts as a conditional, learned attribution generator:

$$F_{\text{zs}} : \mathcal{X} \times \mathbb{R} \rightarrow \mathbb{R}^m, (x, \hat{y}) \mapsto \hat{\phi}, \quad (4)$$

Or, equivalently,

$$\begin{aligned} \hat{\Phi} &= F_{\text{zs}}((X, \hat{Y}) \mid (X_{\text{ref}}, \hat{Y}_{\text{ref}})) := \{\hat{\phi}_1, \dots, \hat{\phi}_n\}, \\ \hat{\phi}_i &= \{\hat{\phi}_i^1, \dots, \hat{\phi}_i^m\} \in \mathbb{R}^m, \end{aligned} \quad (5)$$

Where $\hat{\Phi} \in \mathbb{R}^{n \times m}$ contains the estimated feature-importance vectors for all n instances in X , conditioned on the reference set $(X_{\text{ref}}, \hat{Y}_{\text{ref}})$. The reference set may be any dataset representative of the distribution of interest, including X itself or a subset thereof. Crucially, F_{zs} does not rely on access to f^b . This formalism generalizes the few-shot surrogate model g introduced in Section 3 to the zero-shot setting.

4.1. Tabular Transformer Encoder

To implement the zero-shot mapping defined in Equations (4) and (5), ExplainerPFN uses a transformer encoder (Vaswani et al., 2017) adapted for tabular data, similar to TabPFN. Each pair (x_i, \hat{y}_i) is encoded as a token, producing a d -dimensional embedding that integrates feature values, predicted output, and positional information. Rows interact through multiple layers of bidirectional self-attention, capturing intra- and inter-instance dependencies relevant for feature attribution. The embedding corresponding to the instance being explained after the final layer is used to produce the estimated attribution $\hat{\phi}_i^j$ for each feature.

For a feature j , the input data is reordered to ensure that \hat{y}_i and x_i^j are always in the first two columns of the input matrix before encoding. This allows the model to learn a consistent mapping from the first two columns to the corresponding feature attribution, while still capturing the interactions with the remaining features.

This design allows F_{zs} to accept X and X_{ref} of arbitrary size. However, unlike TabPFN, which masks the labels of test examples during training and inference to simulate the prediction task, ExplainerPFN uses the full (X, \hat{Y}) pairs for all examples in both training and inference. In addition, although ExplainerPFN predicts feature attributions rather than labels, Φ is never used as input.

4.2. Generating Training Data

Training ExplainerPFN requires ground-truth feature importance attributions. However, as discussed in Section 2, exact Shapley values are computationally infeasible to obtain for real-world datasets at scale. To overcome this limitation, we generate all training tasks synthetically and compute ground-truth feature importance. This follows the synthetic prior-fitting paradigm of Hollmann et al. (2025), which we reimplement and adapt for feature attribution by introducing several modifications tailored to predicting Shapley values. A single meta-training task is generated as follows, see Appendix B for details.

1 *Sampling a structural causal model.* We sample a random directed acyclic graph (DAG) representing a structural causal model (SCM), which defines a synthetic tabular data-generating process. Feature values are generated by propagating noise through the graph to obtain a synthetic dataset D , from which we select $m \leq s$ nodes at random to form the input features X and one node to form a binary target Y , and discarding the remaining nodes. This construction yields a dataset consistent with the binary prediction setting described in Section 2. Figure 5a shows an example DAG.

2 *Training a base model.* Next, we define and train f^b . We use a simple feed-forward neural network with one hidden layer of size 100 and ReLU activations. The model is trained on a subset of D for 2000 epochs using the Adam optimizer with initial learning rate $\eta_0 = 0.0001$ and scheduled decay $\eta_t = \frac{\eta_0}{\sqrt{t+1}}$. This yields model predictions $\hat{Y} = f^b(X)$.

3 *Computing ground-truth Shapley values.* Finally, we compute $\phi_i = (\phi_i^1, \dots, \phi_i^m)$ for model f^b over all observations in X using the SHAP framework in Section 2. We apply a hybrid approach that uses exact computation for low-dimensional feature sets and permutation-based SHAP estimation otherwise, yielding a set of feature attributions $\Phi = \{\phi_1, \dots, \phi_n\}$ while keeping computation tractable.

This procedure produces triplets (X, \hat{Y}, Φ) , required for training ExplainerPFN, sampled from a meta-distribution of synthetic tabular tasks. Because the data-generating processes, base model parameters, and target features vary across tasks, ExplainerPFN learns a distribution-level prior over the relationship between (x, \hat{y}) pairs and ϕ .

Finally, to prevent any possibility of data leakage or overfitting to real datasets, ExplainerPFN is trained exclusively on synthetic tasks, and all evaluation is performed on unseen real datasets. The only exception is the DAG-structure experiment in Section D.3, which is conducted on synthetic data by design, to assess structural recovery.

4.3. Training Objective

ExplainerPFN follows the probabilistic training setting of TabPFN but adapts it to the feature-attribution setting. Rather than predicting a scalar output, the model produces a posterior predictive distribution over K discretized “buckets” representing possible values of the standardized attribution:

$$p(\tilde{\phi}_i^j = b_k \mid x_i, \hat{y}_i, X_{\text{ref}}, \hat{Y}_{\text{ref}}), \quad k = 1, \dots, K, \quad (6)$$

The final point estimate used at inference time corresponds to the expectation of this distribution,

$$\hat{\phi}_i^j = \sum_{k=1}^K b_k \cdot p(\tilde{\phi}_i^j = b_k \mid x_i, \hat{y}_i, X_{\text{ref}}, \hat{Y}_{\text{ref}}). \quad (7)$$

Training minimizes the Negative Log Predictive Density:

$$\text{NLPD} = - \sum_{i=1}^n \sum_{j=1}^m \log p(\tilde{\phi}_i^j = b_{k^*} \mid x_i, \hat{y}_i, X_{\text{ref}}, \hat{Y}_{\text{ref}}), \quad (8)$$

where b_{k^*} is the bucket containing the true standardized attribution $\tilde{\phi}_i^j$. NLPD is well established in probabilistic modeling (Candela et al., 2003; Yu et al., 2021), as it encourages both accurate predictions and well-calibrated uncertainty estimates. Optimization uses Adam with cosine-annealed learning rates sampled from $[10^{-7}, 10^{-4}]$, selecting the best-performing schedule based on final training loss.

Since raw Shapley values often have small magnitudes and vary in scale across tasks, we normalize the targets using $\tilde{\phi}_i^j = \frac{\phi_i^j - \mu}{\sigma}$, where μ and σ denote the mean and standard deviation of all Shapley values within a meta-training task. This preserves relative scaling between features while ensuring numerical stability during optimization.

4.4. Improving Attribution Consistency via Shapley Properties

Shapley values are characterized by axioms including symmetry (features that play equivalent roles should receive equivalent attributions) and efficiency (the total attribution equals the model output, up to a baseline) (Shapley, 1953), which impose structural constraints on valid feature attributions. Although ExplainerPFN is trained to predict Shapley values directly, its raw outputs need not satisfy these properties exactly. We use the Shapley axioms as calibration constraints, applying a post-processing step to improve between-feature comparability and explanation fidelity. Each correction below enforces a consequence of the Shapley axioms that can be imposed using only the predicted attributions and model outputs, without access to the underlying model.

Mean-zero attributions (efficiency in expectation). Given X , \hat{Y} , and the base value $v = E[\hat{Y}] = E[f^b(X)]$, we find that $\hat{y}_i = v + \sum_{j=1}^m \phi_i^j$. Using empirical expectations over the dataset as estimators of population expectations gives $E[\hat{Y}] - v = E[\sum_{j=1}^m \phi_i^j] = 0$. Thus, the feature attributions collectively have zero mean across the dataset, $\sum_{i=1}^n \sum_{j=1}^m \phi_i^j = 0$. This allows us to apply a simple re-centering step to the predicted attributions, $\tilde{\phi}_i^j = \hat{\phi}_i^j - \frac{1}{n \cdot m} \sum_{i=1}^n \sum_{j=1}^m \hat{\phi}_i^j$.

Variance decomposition (approximate symmetry via between-feature scaling). SHAP commonly assumes that input features are independent when computing feature attributions. In practice, if we also treat feature attributions as approximately independent (which is consistent with the assumptions in Linear-SHAP (Lundberg & Lee, 2017)), i.e., $\text{Cov}(\phi^a, \phi^b) = 0 \forall \{a, b\} \in M, a \neq b$, then the variance of the model’s predictions can be decomposed

as $Var(\hat{Y}) = \sum_{j=1}^m Var(\phi^j)$. Equivalently, we can consider the expected variance of each feature attribution as $\sigma^2 = \frac{Var(\hat{Y})}{m}$, and standard deviation $\sigma = \frac{Std(\hat{Y})}{\sqrt{m}}$. We rescale the predicted attributions to match the expected per-feature variance,

$$\tilde{\phi}_i^j = \hat{\phi}_i^j \cdot \frac{Std(\hat{Y})/\sqrt{m}}{Std(\hat{\Phi})},$$

where $Std(\hat{\Phi})$ denotes the standard deviation of all predicted attributions in the dataset.

Instance-level efficiency. To ensure $\hat{y}_i = v + \sum_{j=1}^m \tilde{\phi}_i^j$, we introduce an error term ϵ_i , computed as:

$$\hat{y}_i = v + \sum_{j=1}^m [\hat{\phi}_i^j + \epsilon_i] \iff \epsilon_i = \frac{\hat{y}_i - v - \sum_{j=1}^m \hat{\phi}_i^j}{m}, \quad (9)$$

and added to $\tilde{\phi}_i^j$ if no statistical corrections are applied.

Post-processed attributions. Finally, combining all three steps yields the adjusted predicted attributions. We define the partially corrected attributions as:

$$\phi_i^{j,\text{partial}} = \left(\hat{\phi}_i^j - \frac{1}{n \cdot m} \sum_{i=1}^n \sum_{j=1}^m \hat{\phi}_i^j \right) \cdot \frac{Std(\hat{Y})/\sqrt{m}}{Std(\hat{\Phi})}. \quad (10)$$

Over which we apply ϵ_i , *after* the statistical corrections:

$$\tilde{\phi}_i^j = \phi_i^{j,\text{partial}} + \frac{\hat{y}_i - v - \sum_{j=1}^m \phi_i^{j,\text{partial}}}{m}. \quad (11)$$

4.5. Addressing Explanation Multiplicity

Recent work shows that explanations can vary substantially even among models with similar predictive performance, creating challenges for interpretability and robustness (Hwang et al., 2026); see Appendix A for details. To improve robustness against this phenomenon, we diversify the method used for computing ground-truth labels during meta-training. In addition to computing exact Shapley values for a subset of synthetic tasks, we also employ alternative Shapley approximations (e.g., different sampling strategies or random seeds) and vary the initialization of non-parametric base models. While this may introduce variability in the target attributions, it exposes ExplainerPFN to a richer family of attribution patterns, reducing overfitting to any single Shapley-based explainer.

This deliberate variability aims to mitigate explanation multiplicity by encouraging the model to learn stable attribution patterns that generalize across plausible explanation-generating processes, rather than replicating one estimator.

5. Experiments

We evaluate ExplainerPFN under highly limited or absent access to feature attributions. Because true zero-shot Shapley estimators are unavailable, we compare ExplainerPFN’s predictions to SHAP values computed from standard ML models trained with few supervision points, which serve as a practical proxy in low-data regimes.

Datasets. We evaluate ExplainerPFN on 11 tabular datasets from the UCI repository, all unseen during training, and include a real-world case study using the ACS Public Coverage dataset (Ding et al., 2021) (Section 5.4). Additional dataset details are provided in Table 4 in Appendix C.

Base predictors. For each dataset we use two base predictors, f^b , each preceded by a standard scaler (*i.e.*, Z-score normalization): (1) a Multi-Layer Perceptron (MLP) with two hidden layers of size 12 and ReLU activations, and (2) a Random Forest (RF) classifier with 500 estimators. Our goal is not to maximize predictive performance but to use reasonable classifiers with non-linear decision boundaries.

Feature importance predictors. We compare ExplainerPFN against few-shot surrogate explainers trained using small sets of SHAP explanations: a TabPFN regressor, an MLP regressor, and an RF regressor, each trained with 2–10 SHAP examples per dataset. All TabPFN and ExplainerPFN results use a single forward pass without ensembling.

Metrics. We use exact SHAP feature importance values from the base predictors as reference values. Our primary evaluation metric is the Pearson correlation between predicted and reference attributions across instances and features, which captures agreement in relative magnitude and sign. We also report runtime for each method.

Hardware. Experiments were conducted on a machine with a 14-core Intel Xeon Platinum 8268 (2.90GHz) CPU, 32GB RAM, and an NVIDIA V100 GPU with 32GB VRAM.

5.1. Few-shot Feature Importance Estimation

We first examine the performance of few-shot surrogate explainers trained using a small number of SHAP explanations from the target model. Tables 1 and 3 report results for several supervised surrogates trained with 2–10 reference explanations. Notably, few-shot methods, particularly TabPFN-based surrogates, often achieve high correlation with ground-truth SHAP values using as few as two reference observations, with performance improving rapidly as additional supervision becomes available. For example, when using a random forest as the base predictor, TabPFN trained with four reference explanations already achieves correlations of 0.667 on BA and 0.846 on EC, and reaches correlations comparable to or exceeding other surrogates trained with substantially more supervision as the number

Table 1. Pearson correlation between true Shapley values computed based on a RFR (as the base predictor) and estimated Shapley values using ExplainerPFN (zero-shot predictions), as well as a MLP, a RF and TabPFN in different few-shot settings with varying numbers of training samples. Results are reported across a diverse set of UCI datasets.

Method	Samples	BA	AB	AN	CC	EC	FL	GC	HE	HD	HP	TH
EPFN	0	0.898	0.177	0.442	0.479	0.396	0.110	0.161	0.645	0.577	0.645	0.316
MLP	2	-0.060	0.143	-0.002	-0.010	0.052	0.208	0.151	-0.063	0.224	-0.085	0.008
	4	0.017	0.130	0.098	0.076	0.210	0.073	0.157	-0.135	0.067	-0.089	0.022
	6	0.062	-0.060	0.097	0.073	0.317	0.096	0.078	-0.124	0.132	-0.088	0.020
	8	0.657	0.025	0.094	0.090	0.304	0.130	0.116	-0.108	0.200	-0.070	0.025
	10	0.601	-0.063	0.096	0.065	0.405	0.065	0.117	-0.087	0.084	-0.067	0.014
	2	0.373	0.036	0.041	0.134	0.319	0.141	0.050	-0.014	0.220	0.403	0.035
RF	4	0.554	0.090	0.179	0.253	0.517	0.447	0.180	0.265	0.284	0.431	0.095
	6	0.560	0.375	0.276	0.333	0.767	0.583	0.284	0.368	0.314	0.336	0.309
	8	0.766	0.271	0.575	0.353	0.740	<u>0.596</u>	<u>0.288</u>	0.345	0.367	0.417	0.350
	10	0.880	0.283	<u>0.562</u>	0.378	<u>0.961</u>	0.611	0.328	0.402	0.435	0.428	<u>0.594</u>
	2	0.106	0.045	-0.123	0.082	0.211	0.114	0.065	-0.110	-0.062	-0.066	0.035
TabPFN	4	0.667	0.038	0.232	0.527	0.846	0.560	0.155	0.410	0.183	0.483	0.140
	6	0.737	<u>0.294</u>	0.288	0.299	0.941	0.506	0.132	0.394	0.343	0.486	0.326
	8	0.772	0.219	0.517	0.346	0.952	0.351	0.241	0.447	0.386	<u>0.544</u>	0.404
	10	0.903	0.229	0.524	<u>0.447</u>	0.963	0.545	0.244	<u>0.448</u>	<u>0.462</u>	0.526	0.731

of reference explanations increases (0.903 on BA and 0.963 on EC with ten references).

These results demonstrate that high-fidelity feature attributions are attainable even under extremely limited access to explanation supervision. This few-shot regime provides a useful reference point for evaluating zero-shot methods, which we consider next.

5.2. Zero-shot Feature Importance Estimation

We evaluate ExplainerPFN in a true zero-shot setting, where no access is available to the base predictor f^b or to reference SHAP explanations. We compare ExplainerPFN against three few-shot surrogate explainers trained with 2–10 SHAP explanations from the base predictor. This comparison is intentionally stringent: while ExplainerPFN operates without supervision, the baselines benefit from direct access to exact Shapley values from the target model.

Table 1 reports results using a RF as f^b . ExplainerPFN achieves competitive performance across most datasets, attaining the highest correlation with SHAP on 4 of 11 datasets and second-best performance on BA. These results indicate that meaningful attribution structure can be recovered from the data distribution alone, even without model access. ExplainerPFN also consistently outperforms MLP-based surrogate explainers across nearly all configurations. We extend this analysis to MLP base predictors in Appendix D, both for completeness and to further explore explanation multiplicity discussed in Section 4.5.

Best- and worst-case zero-shot behavior. We analyze ExplainerPFN’s behavior in representative best- and worst-

case scenarios identified in Table 5, using RF as the base model. Figure 1a shows results on the AB dataset, where ExplainerPFN performs poorly. While the method captures the relative ordering of feature importance, it fails to accurately recover absolute magnitudes, leading to overestimation of a negatively contributing feature and a distorted

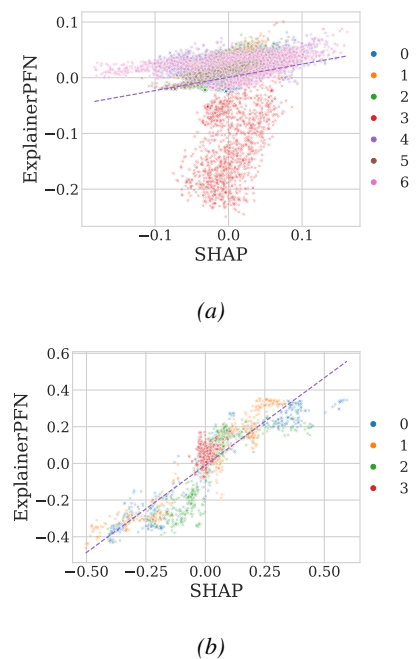


Figure 1. Comparison between ExplainerPFN and SHAP feature-importance attributions across the worst and best performing cases for ExplainerPFN, using the RF as base model: (a) Abalone (AB) and (b) Banknote Authentication (BA).

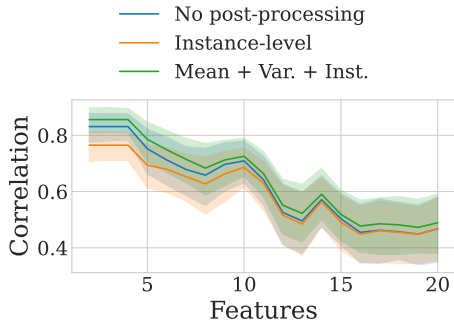


Figure 2. Pearson correlation analysis between ExplainerPFN and SHAP feature importance attribution on synthetic datasets, as a function of the number of features using different correction steps. On average, no post-processing (blue) outperforms instance-level efficiency correction (orange), but both are consistently outperformed by applying all correction steps (green; mean-zero attributions, variance decomposition, and instance-level efficiency).

attribution distribution after post-processing. In contrast, Figure 1b shows results on the BA dataset, where ExplainerPFN closely aligns with SHAP both in relative ordering and absolute magnitude. This comparison highlights both the current limitations of zero-shot estimation, particularly in between-feature scaling, and its potential to produce accurate explanations when data characteristics are favorable.

Effect of Shapley-consistent post-processing. We analyze the impact of the post-processing steps in Section 4.4 on zero-shot performance using synthetic datasets with ground-truth Shapley values, shown in Figure 2, and extend this discussion in Appendix E. While raw ExplainerPFN outputs capture meaningful attribution structure, applying the full post-processing pipeline consistently improves alignment with ground-truth Shapley values compared to raw outputs or partial corrections. The mean-zero and variance-based scaling steps help align the scale and offset of predicted attributions, which in turn enhances the effectiveness of the instance-level efficiency correction. However, we also find that ExplainerPFN outputs tend to degrade as feature dimensionality increases.

Robustness to explanation multiplicity. We assess robustness to explanation multiplicity by evaluating zero-shot performance across different base predictors. Following the evaluation guidance of (Hwang et al., 2026), we repeat the zero-shot experiments using a multi-layer perceptron as the base model instead of a random forest (Appendix D.1). Despite differences in model architecture and the resulting SHAP explanations, ExplainerPFN exhibits similar performance trends across base predictors, maintaining competitive correlation with ground-truth Shapley values on multiple datasets. This consistency indicates that ExplainerPFN does not overfit to a single explanation-generating process,

Table 2. Average computation time (in seconds) for estimating 1000 feature contributions using different methods across all tested datasets. Inference times for TabPFN, MLP and RF are reported for 10-shot settings and include the cost of computing SHAP values for the supervision samples.

Method	Base Model	
	MLP	RF
SHAP	0.234	8.498
ExplainerPFN	0.876	0.793
TabPFN	1.599	2.362
MLP	0.106	0.800
RF	1.317	2.026

and that the training-time diversification strategy described in Section 4.5 contributes to robustness under explanation multiplicity. Additional analyses isolating explanation-side variability are provided in Appendix D.

5.3. Computational Efficiency

Beyond accuracy, computational efficiency is a critical consideration for practical deployment of feature attribution methods. Table 2 shows a significant gap between SHAP and the learned estimators, with the magnitude of this gap strongly dependent on the base predictor’s complexity. When the base predictor is a small MLP, SHAP achieves the second fastest computation time (0.234s), outperformed by the MLP surrogate (0.106s). For small neural networks, the cost of forward passes during SHAP’s sampling procedure remains low. However, as the base predictor complexity increases to a RF with 500 estimators, SHAP’s computation time increases to ≈ 8.5 seconds, a $36\times$ slowdown. In contrast, ExplainerPFN’s inference time depends only on the input data. As a result, its inference time remains nearly constant across both base predictors, representing $>10\times$ speedup over SHAP when explaining RF predictions.

These results reveal an accuracy-efficiency trade-off. ExplainerPFN achieves zero-shot performance frequently superior to 4-6 shot surrogate explainers (see Tables 1 and 3), while maintaining inference speed comparable to or faster than methods that rely on supervised SHAP examples. While SHAP provides high-quality estimations when the base model has reduced inference time and accessible, ExplainerPFN offers a practical alternative for scenarios where computational resources are limited, model access is restricted, or real-time explanations are required.

5.4. Case study: ACS Public Coverage

We evaluate ExplainerPFN on ACS Public Coverage from the 2018 1-Year American Community Survey for Alabama (Ding et al., 2021), accessed via the `folktables` library. The task is to predict public health insurance cov-

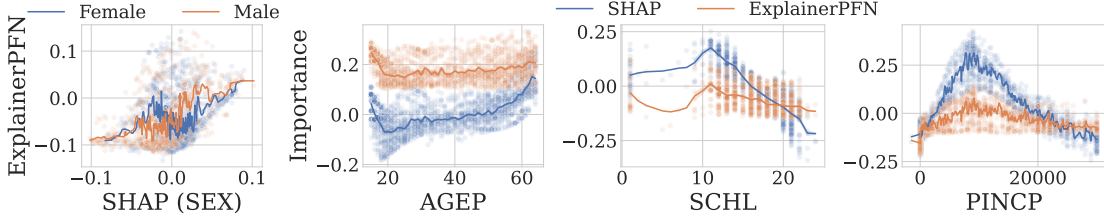


Figure 3. Per-feature comparison between ExplainerPFN and SHAP’s feature importance attributions for predicting health insurance coverage using the ACS Public Coverage dataset.

verage (PCOV) using four features: age (AGEP), education (SCHL), income (PINCP), and sex (SEX). We use stratified training and test splits of 2,000 samples each. This is a challenging case for ExplainerPFN, with a Pearson correlation of 0.32 relative to SHAP, placing it at the lower end of the performance range observed in Section 5.2. Examining such cases helps clarify the method’s limitations.

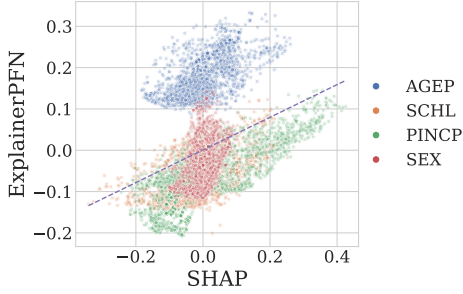


Figure 4. Overall comparison between ExplainerPFN and SHAP’s feature importance attributions for predicting health insurance coverage in the ACS Public Coverage dataset.

Figure 3 compares per-feature attributions from ExplainerPFN and SHAP. Although the methods differ in scale, ExplainerPFN recovers consistent directional patterns. Figure 4 further compares SHAP and ExplainerPFN values across all features and instances: SCHL and PINCP show strong linear agreement, indicating consistent importance and effect direction, while SEX exhibits weaker but still positive alignment. AGEP shows the largest discrepancy, with consistent sign but an overestimation of contribution magnitudes by ExplainerPFN relative to SHAP.

6. Limitations and Future Work

We showed that feature importance can be estimated in a zero-shot, model-free setting, but our experiments also surface limitations that suggest clear next steps.

Cross-feature calibration. ExplainerPFN recovers relative ordering and directional effects, but can misestimate abso-

lute magnitudes across features. Improving calibration by separating within-feature trend estimation from between-feature scale and offset is an important future direction.

Scaling with dimensionality and interactions. Zero-shot quality degrades as feature dimensionality grows and interactions become more complex. Future work should explore architectures that are more robust in high-dimensional regimes and better capture interaction effects.

Synthetic-to-real transfer and coverage. Training exclusively on synthetic tasks prevents leakage but may not capture key properties of real tabular data. Enriching the synthetic generator, evaluating robustness under distribution shift, and extending to mixed-type tables and broader prediction tasks, would improve applicability.

Our results suggest a useful decomposition of the zero-shot attribution problem into three subproblems: within-feature estimation (recovering directional or functional trends), between-feature estimation (recovering comparable scales across features), and decomposing feature contributions (separating trend from scale). Making this decomposition explicit may yield more reliable zero-shot explanations.

7. Conclusion

We introduced the task of zero-shot, model-free feature importance estimation and proposed ExplainerPFN, a tabular foundation model that predicts Shapley-style feature attributions from input-prediction pairs without access to the underlying model or reference explanations. Across a range of real and synthetic datasets, ExplainerPFN achieves competitive performance relative to few-shot surrogate explainers while providing substantial computational savings when model access is limited or SHAP computation is costly. Together, our results suggest that meaningful attribution structure can be recovered from the data distribution alone, and point to a promising direction for scalable, model-free explainability in tabular settings.

Impact Statement

We introduce the task of zero-shot, model-free feature importance estimation and propose a Tabular Foundation Model that produces Shapley-like explanations without requiring access to the underlying predictive model. By enabling explanations in settings where the model cannot be inspected directly, this work aims to expand the practical reach of explainable AI. Potential positive impacts include greater transparency in automated decision systems, facilitating preliminary audits for fairness and bias when internal models are inaccessible, and reducing the computational burden associated with traditional Shapley value computation in large-scale applications. We view these explanations primarily as a triage tool under realistic access constraints, not as a substitute for model-access explanation methods when those are available.

However, we also acknowledge important limitations and potential risks. Because ExplainerPFN operates without model access, its attributions are approximate and may not reflect the true causal behavior of specific underlying models. Users may misinterpret these explanations if they assume they are exact, leading to overconfidence in conclusions about model behavior. The method may also yield less reliable results in high-dimensional settings or in domains where the synthetic pretraining distribution fails to capture critical real-world structure, potentially limiting its applicability without further adaptation. In high-stakes settings, approximate attributions could also be misused as evidence of compliance or fairness without appropriate validation.

Broader deployment of zero-shot explainability techniques should be accompanied by efforts to understand and document their appropriate use cases and limitations. Future research could explore formal guarantees, robustness under distribution shift, and best practices for integrating such tools into responsible ML pipelines. When possible, we recommend validating key findings against model-access explanations and reporting sensitivity indicators (e.g., stability across reference sets or seeds) to reduce the risk of overinterpretation. This method does not solve all challenges of transparent decision-making, but we hope it encourages further investigation into explanation methods that are practical and informative under realistic access constraints.

To promote future research in this challenging, societally beneficial direction, we release all the artifacts (code, models, data, benchmarks, etc.) produced during this work.

8. Acknowledgments

This work was supported in part by US National Science Foundation (NSF) Awards No. 2312930, 2326193. This work was also supported in part by the NYU-KAIST Partnership and by the Institute of Information & Communi-

cations Technology Planning & Evaluation (IITP) with a grant funded by the Ministry of Science and ICT (MSIT) of the Republic of Korea in connection with the Global AI Frontier Lab International Collaborative Research. (No. RS-2024-00469482 & RS-2024-00509258). This work was also supported in part by the European Union’s Horizon Europe research and innovation program under Grant Agreement No. 101189689, and by Fundação para a Ciência e a Tecnologia, I.P. (FCT) under projects UID/50021/2025 (DOI: <https://doi.org/10.54499/UID/50021/2025>) and UID/PRR/50021/2025 (DOI: <https://doi.org/10.54499/UID/PRR/50021/2025>).

References

Achille, A., Lam, M., Tewari, R., Ravichandran, A., Maji, S., Fowlkes, C. C., Soatto, S., and Perona, P. Task2vec: Task embedding for meta-learning. In *Proceedings of the IEEE/CVF international conference on computer vision*, pp. 6430–6439, 2019.

Arenas, M., Barcelo, P., Bertossi, L., and Monet, M. On the complexity of shap-score-based explanations: Tractability via knowledge compilation and non-approximability results. *Journal of Machine Learning Research*, 24(63):1–58, 2023. URL <http://jmlr.org/papers/v24/21-0389.html>.

Black, E., Raghavan, M., and Barocas, S. Model multiplicity: Opportunities, concerns, and solutions. In *Proceedings of the 2022 ACM Conference on Fairness, Accountability, and Transparency*, FAccT ’22, pp. 850–863, New York, NY, USA, 2022. Association for Computing Machinery. ISBN 9781450393522. doi: 10.1145/3531146.3533149. URL <https://doi.org/10.1145/3531146.3533149>.

Brown, T., Mann, B., Ryder, N., Subbiah, M., Kaplan, J. D., Dhariwal, P., Neelakantan, A., Shyam, P., Sastry, G., Askell, A., et al. Language models are few-shot learners. *Advances in neural information processing systems*, 33: 1877–1901, 2020.

Candela, J. Q., Girard, A., Larsen, J., and Rasmussen, C. E. Propagation of uncertainty in bayesian kernel models—application to multiple-step ahead forecasting. In *2003 IEEE International Conference on Acoustics, Speech, and Signal Processing, 2003. Proceedings.(ICASSP’03)*, volume 2, pp. II–701. IEEE, 2003.

Cheng, Q., Xing, J., Xue, C., and Yang, X. Unifying Prediction and Explanation in Time-Series Transformers via Shapley-based Pretraining, January 2025. URL <http://arxiv.org/abs/2501.15070>. arXiv:2501.15070 [cs].

Ding, F., Hardt, M., Miller, J., and Schmidt, L. Retiring adult: New datasets for fair machine learning. *Advances in neural information processing systems*, 34:6478–6490, 2021.

Dugas, C., Bengio, Y., Bélisle, F., Nadeau, C., and Garcia, R. Incorporating second-order functional knowledge for better option pricing. *Advances in neural information processing systems*, 13, 2000.

Finn, C., Abbeel, P., and Levine, S. Model-agnostic meta-learning for fast adaptation of deep networks. In Precup, D. and Teh, Y. W. (eds.), *Proceedings of the 34th International Conference on Machine Learning*, volume 70 of *Proceedings of Machine Learning Research*, pp. 1126–1135. PMLR, 06–11 Aug 2017. URL <https://proceedings.mlr.press/v70/finn17a.html>.

Gorishniy, Y., Rubachev, I., Khrulkov, V., and Babenko, A. Revisiting deep learning models for tabular data. *Advances in neural information processing systems*, 34: 18932–18943, 2021.

Gurung, R., Ragodos, R., Ma, C., Wang, T., and Chen, C. Protopairnet: Interpretable regression through prototypical pair reasoning. In *The Thirty-ninth Annual Conference on Neural Information Processing Systems*.

Hegselmann, S., Buendia, A., Lang, H., Agrawal, M., Jiang, X., and Sontag, D. Tabllm: Few-shot classification of tabular data with large language models. In Ruiz, F., Dy, J., and van de Meent, J.-W. (eds.), *Proceedings of The 26th International Conference on Artificial Intelligence and Statistics*, volume 206 of *Proceedings of Machine Learning Research*, pp. 5549–5581. PMLR, 25–27 Apr 2023. URL <https://proceedings.mlr.press/v206/hegselmann23a.html>.

Hod, S., Rosenblatt, L., and Stoyanovich, J. Do you really need public data? surrogate public data for differential privacy on tabular data. In *1st ICML Workshop on Foundation Models for Structured Data*, 2025.

Hollmann, N., Müller, S., Eggensperger, K., and Hutter, F. Tabpfn: A transformer that solves small tabular classification problems in a second. In *The Eleventh International Conference on Learning Representations*, 2023.

Hollmann, N., Müller, S., Purucker, L., Krishnakumar, A., Körfer, M., Hoo, S. B., Schirrmeister, R. T., and Hutter, F. Accurate predictions on small data with a tabular foundation model. *Nature*, 637(8045):319–326, 2025.

Huang, X., Khetan, A., Cvitkovic, M., and Karnin, Z. Tab-transformer: Tabular data modeling using contextual embeddings. *arXiv preprint arXiv:2012.06678*, 2020.

Hwang, H., Bell, A., Fonseca, J., Pliatsika, V., Stoyanovich, J., and Whang, S. E. Shap-based explanations are sensitive to feature representation. In *Proceedings of the 2025 ACM Conference on Fairness, Accountability, and Transparency*, pp. 1588–1601, 2025.

Hwang, H., Lee, S., Rosenblatt, L., Whang, S. E., and Stoyanovich, J. Explanation multiplicity in SHAP: Characterization and assessment, 2026. URL <https://arxiv.org/abs/2601.12654>.

Kobylińska, K., Krzyziński, M., Machowicz, R., Adamek, M., and Biecek, P. Exploration of the rashomon set assists trustworthy explanations for medical data. *IEEE Journal of Biomedical and Health Informatics*, 28(11): 6454–6465, 2024.

Kotelnikov, A., Baranchuk, D., Rubachev, I., and Babenko, A. Tabddpm: Modelling tabular data with diffusion models. In *International conference on machine learning*, pp. 17564–17579. PMLR, 2023.

Krapivsky, P. L. and Redner, S. Organization of growing random networks. *Phys. Rev. E*, 63: 066123, May 2001. doi: 10.1103/PhysRevE.63.066123. URL <https://link.aps.org/doi/10.1103/PhysRevE.63.066123>.

Kumaraswamy, P. A generalized probability density function for double-bounded random processes. *Journal of hydrology*, 46(1-2):79–88, 1980.

Lei, J., G’Sell, M., Rinaldo, A., Tibshirani, R. J., and Wasserman, L. Distribution-free predictive inference for regression. *Journal of the American Statistical Association*, 113(523):1094–1111, 2018.

Lundberg, S. M. and Lee, S.-I. A unified approach to interpreting model predictions. Curran Associates, Inc., 2017.

Lundberg, S. M., Erion, G., Chen, H., DeGrave, A., Prutkin, J. M., Nair, B., Katz, R., Himmelfarb, J., Bansal, N., and Lee, S.-I. From local explanations to global understanding with explainable ai for trees. *Nature machine intelligence*, 2(1):56–67, 2020.

Ma, J., Thomas, V., Hosseinzadeh, R., Labach, A., Cresswell, J. C., Golestan, K., Yu, G., Caterini, A. L., and Volkovs, M. Tabdpt: Scaling tabular foundation models on real data. In *The Thirty-ninth Annual Conference on Neural Information Processing Systems*, 2025.

Mitchell, R., Cooper, J., Frank, E., and Holmes, G. Sampling permutations for shapley value estimation. *Journal of Machine Learning Research*, 23(43):1–46, 2022.

Naik, D. K. and Mammone, R. J. Meta-neural networks that learn by learning. In *[Proceedings 1992] IJCNN International Joint Conference on Neural Networks*, volume 1, pp. 437–442. IEEE, 1992.

Pliatsika, V., Fonseca, J., Akhynko, K., Shevchenko, I., and Stoyanovich, J. Sharp: Explaining rankings and preferences with shapley values. *Proceedings of the VLDB Endowment*, 18(11):4131–4143, 2025.

Schmidhuber, J. *Evolutionary principles in self-referential learning, or on learning how to learn: the meta-meta... hook*. PhD thesis, Technische Universität München, 1987.

Shapley, L. S. A value for n-person games. 1953.

Shi, J., Xu, M., Hua, H., Zhang, H., Ermon, S., and Leskovec, J. Tabdiff: a mixed-type diffusion model for tabular data generation. In *The Thirteenth International Conference on Learning Representations*, 2025.

Škrlić, B., Džeroski, S., Lavrač, N., and Petković, M. Feature importance estimation with self-attention networks. *arXiv preprint arXiv:2002.04464*, 2020.

Slack, D., Hilgard, A., Lakkaraju, H., and Singh, S. Counterfactual explanations can be manipulated. *Advances in neural information processing systems*, 34:62–75, 2021.

Snell, J., Swersky, K., and Zemel, R. Prototypical networks for few-shot learning. *Advances in neural information processing systems*, 30, 2017.

Somepalli, G., Goldblum, M., Schwarzschild, A., Bruss, C. B., and Goldstein, T. Saint: Improved neural networks for tabular data via row attention and contrastive pre-training. *arXiv preprint arXiv:2106.01342*, 2021.

Thrun, S. and Pratt, L. Learning to learn: Introduction and overview. In *Learning to learn*, pp. 3–17. Springer, 1998.

Van Breugel, B. and Van Der Schaar, M. Position: Why tabular foundation models should be a research priority. In Salakhutdinov, R., Kolter, Z., Heller, K., Weller, A., Oliver, N., Scarlett, J., and Berkenkamp, F. (eds.), *Proceedings of the 41st International Conference on Machine Learning*, volume 235 of *Proceedings of Machine Learning Research*, pp. 48976–48993. PMLR, 21–27 Jul 2024. URL <https://proceedings.mlr.press/v235/van-breugel24a.html>.

van Breugel, B., Crabbé, J., Davis, R., and van der Schaar, M. Latable: Towards large tabular models. *arXiv preprint arXiv:2406.17673*, 2024.

Vaswani, A., Shazeer, N., Parmar, N., Uszkoreit, J., Jones, L., Gomez, A. N., Kaiser, Ł., and Polosukhin, I. Attention is all you need. *Advances in neural information processing systems*, 30, 2017.

Verdinelli, I. and Wasserman, L. Feature importance: A closer look at shapley values and loco. *Statistical Science*, 39(4):623–636, 2024.

Villaizán-Vallelado, M., Salvatori, M., Segura, C., and Arapakis, I. Diffusion models for tabular data imputation and synthetic data generation. *ACM Transactions on Knowledge Discovery from Data*, 19(6):1–32, 2025.

Williamson, B. D., Gilbert, P. B., Carone, M., and Simon, N. Nonparametric variable importance assessment using machine learning techniques. *Biometrics*, 77(1):9–22, 2021.

Williamson, B. D., Gilbert, P. B., Simon, N. R., and Carone, M. A general framework for inference on algorithm-agnostic variable importance. *Journal of the American Statistical Association*, 118(543):1645–1658, 2023.

Wu, Y. and Bergman, D. L. Zero-shot meta-learning for tabular prediction tasks with adversarially pre-trained transformer. In *Forty-second International Conference on Machine Learning*, 2025. URL <https://openreview.net/forum?id=q91ITFNKds>.

Xin, R., Zhong, C., Chen, Z., Takagi, T., Seltzer, M., and Rudin, C. Exploring the whole rashomon set of sparse decision trees. *Advances in neural information processing systems*, 35:14071–14084, 2022.

Yu, Z., Zhu, M., Trapp, M., Skryagin, A., and Kersting, K. Leveraging probabilistic circuits for nonparametric multi-output regression. In de Campos, C. and Maathuis, M. H. (eds.), *Proceedings of the Thirty-Seventh Conference on Uncertainty in Artificial Intelligence*, volume 161 of *Proceedings of Machine Learning Research*, pp. 2008–2018. PMLR, 27–30 Jul 2021. URL <https://proceedings.mlr.press/v161/yu21a.html>.

Zheng, S. and Charoenphakdee, N. Diffusion models for missing value imputation in tabular data. In *NeurIPS 2022 First Table Representation Workshop*, 2022. URL <https://openreview.net/forum?id=4q9kFrXC2Ae>.

A. Related Work

Transformers for tabular data. Earlier works, such as SAINT (Somepalli et al., 2021), TabTransformer (Huang et al., 2020), and FT-Transformer (Gorishniy et al., 2021), have adapted the transformer architecture for supervised learning on tabular data. These models typically employ self-attention mechanisms to attend to both individual features within each observation and across different observations in the dataset. These models are designed for supervised learning on a single dataset and require fine-tuning on new datasets.

Tabular foundation models. Recent advances in foundation models for tabular data have demonstrated the effectiveness of large pretrained architectures for supervised learning tasks on tabular data. Early work in this direction includes TabPFN (Hollmann et al., 2023), which frames tabular prediction as a sequence modeling problem and trains a transformer to emulate the Bayesian inference procedure of a neural process. A refined and more accurate iteration of TabPFN (Hollmann et al., 2025) extends the original formulation in several ways, particularly support for regression tasks and greater robustness to unimportant features and outliers. Other recent approaches such as LaTable (van Breugel et al., 2024) adopt a diffusion-based approach that incorporates dataset descriptions and column names to improve its generative accuracy. More recently, TabDPT (Ma et al., 2025) achieved strong downstream performance on unseen regression and classification benchmarks via self-supervised learning (SSL).

Diffusion models for tabular data generation. TabDiff (Shi et al., 2025) is a diffusion-based model for generating tabular data. It uses a transformer-based architecture to model the denoising process. However, TabDiff requires re-training on each new dataset, making it unsuitable for zero-shot learning scenarios. Similarly, MTabGen (Villaizán-Vallelado et al., 2025) is a diffusion model for data imputation and synthetic data generation on tabular data, which generalizes TabDDPM (Kotelnikov et al., 2023). Other methods, such as TabCSDI (Zheng & Charoenphakdee, 2022), are aimed towards handling missing value imputation in tabular data by supporting both numerical and categorical variables. However, to the best of our knowledge, none of these diffusion models are designed for in-context learning.

Network-based feature importance estimation. Škrlj et al. (2020) propose a Self-Attention Network that generates feature importance scores alongside predictions. However, it must be trained over each target dataset to predict the target feature and the explanations correspond to the attention weights over features. In practice, this approach explains a secondary model’s internal attention mechanism, whose predictions and explanation may not align with feature importance of the base model’s predictions. More recently,

Cheng et al. (2025) proposed ShapTST, a framework that integrates Shapley value-based explanation generation directly into time-series transformer training. This enables models to output both predictions and feature importance explanations in a single forward pass. However, ShapTST is specifically designed for time-series data, and requires retraining for each new dataset, along with computation of Shapley values (or approximations thereof) during training. To the best of our knowledge, our work is the first to propose a tabular foundation model that generates feature importance explanations in a zero-shot manner without retraining on new datasets.

Meta-learning for tabular data. Meta-learning exposes models to many small tabular tasks, enabling generalization to new tasks (Thrun & Pratt, 1998; Schmidhuber, 1987; Naik & Mammone, 1992). MAML (Finn et al., 2017) is a popular model-agnostic training algorithm (a meta-learning procedure) that learns a good initialization for the underlying model. However, this approach requires fine-tuning on new tasks, making it unsuitable for zero-shot learning scenarios. Prototypical Networks (Snell et al., 2017) learn an embedding space where each class is represented by the mean (prototype) of its few labeled examples, and classification is done by nearest prototype using a distance-based softmax. This method is extended for zero-shot learning, but for both the few-shot and zero-shot setting, this method still requires gradient updates on new tasks and is exclusive for classification. Recent work has extended this approach to regression tasks (Gurung et al.). Task2Vec (Achille et al., 2019) represents each supervised visual classification task as a fixed-length vector. It allows for measuring task similarity and selecting the best pretrained model for a new task. However, this method assumes access to different pretrained models, which are scarce for tabular data.

Zero-shot Learning on tabular data. TabLLM explores the application of large language models to zero-shot and few-shot classification of tabular data (Hegselmann et al., 2023). TabPFN shows strong few-shot performance on tabular data by pretraining on a large number of synthetic datasets (Hollmann et al., 2023). LaTable demonstrates potential for zero-shot classification results by leveraging dataset and column descriptions (van Breugel et al., 2024). Prior works such as (Wu & Bergman, 2025) focus on zero-shot meta learning, they use the term to refer to models that perform predictions on unseen datasets with zero gradient update on the model, and with no reliance on the context similarity between this dataset and the datasets that the model was pre-trained on. However, this concept diverges from the typical zero-shot learning. In our work, zero-shot learning refers to the amount of empirical examples for prediction being zero.

Model-free feature importance. Model-free feature im-

portance methods aim to quantify the contribution of each feature without relying on a fitted predictive model, distinguishing them from model-agnostic methods that still require model evaluations. A central example is the Leave-One-Covariate-Out (LOCO) framework of Lei et al. (2018), which measures a feature’s importance by assessing how predictive performance changes when that feature is removed from the dataset. However, LOCO is only able to provide global feature contributions and still requires knowledge about the base model in order to train comparable surrogate models without the feature of interest. Subsequent work has refined this idea: Verdinelli & Wasserman (2024) provide improved statistical guarantees and broaden the applicability of LOCO-style estimators, while Williamson et al. (2023) introduce a generalized formulation that incorporates a data-splitting strategy to yield more stable and interpretable importance estimates. Extending the LOCO intuition beyond any specific model class, Williamson et al. (2021) propose a nonparametric variable-importance measure that uses cross-fitting and influence-function theory to deliver unbiased global estimates and confidence intervals.

Explanation Multiplicity. Hwang et al. (2025) show that SHAP-based feature importance explanations are sensitive to feature representation and simple preprocessing choices, indicating that explanation methods themselves are unstable to seemingly innocuous changes in input encoding. Similarly, Slack et al. (2021) demonstrate that counterfactual explanations are highly sensitive to input perturbations and can be manipulated, revealing that explanations may not be reliable under predictive multiplicity and can conceal model biases even when test accuracy is unchanged. More broadly, the model multiplicity phenomenon has been formalized and explored across several studies. Black et al. (2022) define and analyze model multiplicity, showing there can exist many predictively equivalent models with different decision boundaries, which has important implications for fairness, arbitrariness, and recourse. In the context of specific model classes, Xin et al. (2022) develop methods to enumerate the Rashomon set of sparse decision trees, making it possible to inspect the full set of nearly equally good models rather than selecting only one. Building on this, Kobylińska et al. (2024) show that it is possible to identify models with substantially different behavior by exploring the Rashomon set, which helps generate more trustworthy explanations in high-stakes domains like medical data analysis. Together, these works illustrate both the risks of relying on a single model/explanation and the opportunities afforded by explicitly considering model and explanation multiplicity when building and interpreting machine learning systems.

B. Additional details on training data generation

This section extends Section 4.2 with additional details on the synthetic data generation process used to train ExplainerPFN. In particular, we describe the procedure used to sample directed acyclic graphs (DAGs), the distributions employed to generate values for exogenous (base) nodes, and the propagation mechanisms used to compute values for downstream nodes.

DAG Sampling. To generate structural dependencies among features, we sample directed acyclic graphs (DAGs) using the Growing Network with Redirection (GNR) procedure (Krapivsky & Redner, 2001), which produces sparse, scale-free graph topologies. In this framework, nodes are added sequentially; each new node selects an existing node uniformly at random and either attaches to it directly or, with probability p , sampled from either a gamma or uniform distribution, redirects the edge to that node’s parent. This process naturally induces heterogeneous in-degree distributions and a mixture of shallow and deep dependency chains, providing diverse structural patterns for pretraining. The number of nodes N is sampled from a uniform distribution over a user-specified range (we chose $[2, 10]$), while the redirection probability p is drawn from a Gamma distribution, allowing control over the expected sparsity of the resulting DAG. We also allow for the generation of multiple, small, disconnected subgraphs, generated as described previously, which are then connected following GNR procedure. When selecting the target node and input features, we allow for the possibility that some features may be disconnected from the target node (i.e., belong to different subgraphs). This reflects real-world scenarios where some features may be non-informative for the learning task.

Edge mappings. Each edge in the sampled DAG is associated with a nonlinear activation used when propagating values from parent to child nodes. We draw these activation functions uniformly from a diverse set to encourage non-trivial feature interactions: identity, logarithm, sigmoid, absolute value, sine, hyperbolic tangent, rank transformation, square and power functions, SmoothReLU/Softplus (Dugas et al., 2000), step, and modulo operations.

Computational considerations. Due to the computational overhead introduced with the training of a ML classifier, as well as computation of Shapley values for each classifier and synthetic dataset, the synthetic data generation process cannot be done online (i.e., as the model is being trained). Therefore, we generate data in parallel to the model training; we instantiated two VMs, where one is generating and saving data, while the other is sampling data from the generation process. This means ExplainerPFN can repeatedly sample the same synthetic datasets over the generation process. We attempted to mitigate this issue via the generation

of large amounts of data (hundreds of thousands of datasets).

Future work. We note that the current generator uses only a fixed family of edge mappings. As part of future work, we plan to expand this library to incorporate additional distributional transformations (e.g., Kumaraswamy distortions (Kumaraswamy, 1980), rule-based dependencies, etc.) and more complex base node sampling mechanisms to account for between-observation dependencies, to further increase the quality of the synthetic datasets. In addition, we plan to explore other mechanisms to mitigate some of the computational overhead introduced by the data generation process.

C. Additional information on Datasets used

This section provides supplementary details on the datasets used in our experiments, including data sources, preprocessing steps, and task-specific adjustments. Throughout all experiments and preprocessing steps over all the stages of development of this research, we used a fixed random seed (42).

C.1. Tabular Benchmark Datasets

We evaluate ExplainerPFN on a collection of tabular binary classification tasks, focusing on continuous features. For datasets with originally multiclass classification tasks, we convert the task to binary classification using a majority-vs-rest scheme. To maintain consistency with TabPFN-style problem settings and ExplainerPFN’s training scheme, we retain only datasets satisfying $2 < m < 15$ and $n < 20,000$.

During evaluation, modeling pipelines include a standard scaler before fitting the downstream classifier or regressor. Shapley values are computed on the scaled feature representations, since the SHAP framework does not support explanations over the raw input data under certain scenarios.

C.2. ACS Public Coverage Case Study

For the ACS case study, we use the 2018 American Community Survey (ACS) data for Alabama, accessed via the folktypes interface (Ding et al., 2021). We restrict the feature set to AGEP, SCHL, PINCP, and SEX to facilitate analysis while retaining sensitive attributes. The dataset is split into a training and test set, both with 2000 samples. We train a pipeline consisting of a standard scaler, followed by a tuned MLP. SHAP values are computed on the fitted model, while ExplainerPFN uses the concatenated train and test feature matrix, along with the model’s scores.

Table 3. Pearson correlation between true Shapley values computed based on a MLP (as the base predictor) and estimated Shapley values using ExplainerPFN (zero-shot predictions), as well as a MLP, a RF and TabPFN in different few-shot settings with varying numbers of training samples. Results are reported across a diverse set of UCI datasets.

Method	Samples	BA	AB	AN	CC	EC	FL	GC	HE	HD	HP	TH
MLP	0	0.880	0.117	0.334	0.529	0.478	0.064	0.221	0.473	0.554	0.515	0.211
	2	-0.054	-0.006	-0.046	0.035	0.064	0.104	0.178	-0.123	0.203	-0.030	0.009
	4	0.024	0.221	0.161	0.064	0.206	0.057	0.155	-0.164	0.048	0.044	0.019
	6	0.083	0.154	0.159	0.051	0.353	0.151	0.105	-0.144	0.111	0.025	0.018
	8	0.743	0.180	0.159	0.077	0.312	0.175	0.167	-0.128	0.184	0.039	0.022
	10	0.734	0.143	0.160	0.075	0.424	0.164	0.149	-0.122	0.073	0.040	0.013
RF	2	0.201	0.019	0.029	0.166	0.191	0.107	0.059	-0.113	0.172	-0.002	0.054
	4	0.359	0.090	0.050	0.314	0.356	0.261	0.220	0.166	0.212	0.026	0.121
	6	0.433	0.627	0.172	0.275	0.729	0.383	0.312	0.255	0.261	0.019	0.341
	8	0.775	0.687	0.261	0.454	0.682	0.419	0.342	0.332	0.386	0.039	0.372
	10	0.831	<u>0.684</u>	<u>0.288</u>	<u>0.563</u>	0.904	<u>0.466</u>	0.356	0.393	<u>0.457</u>	0.036	<u>0.608</u>
TabPFN	2	0.066	0.020	0.031	0.062	0.076	0.059	0.053	-0.138	0.004	-0.014	0.051
	4	0.712	0.147	0.018	0.633	0.792	0.401	0.282	0.170	0.327	0.042	0.143
	6	0.837	0.599	0.063	0.441	0.900	<u>0.466</u>	0.259	0.398	0.357	0.065	0.329
	8	<u>0.903</u>	0.606	0.155	0.517	<u>0.910</u>	0.452	<u>0.367</u>	<u>0.518</u>	0.428	<u>0.091</u>	0.345
	10	0.956	0.643	0.166	0.791	0.923	0.504	0.444	0.539	0.217	0.078	0.693

Table 4. Summary of datasets used in experiments.

Dataset name	Obs.	Feat.	Maj./Min.	IR
Echocardiogram (EC)	61	8	44/17	2.59
Hepatitis (HP)	129	4	105/24	4.38
Flags (FL)	194	10	134/60	2.23
Heart (HE)	270	6	150/120	1.25
Heart Disease (HD)	740	5	383/357	1.07
Annealing (AN)	798	6	608/190	3.20
German Credit (GC)	1000	7	700/300	2.33
Banknote Auth. (BA)	1372	4	762/610	1.25
Contraceptive (CC)	1473	5	844/629	1.34
Abalone (AB)	4177	7	3488/689	5.06
Thyroid (TH)	5789	6	4168/1621	2.57

C.3. DAG Recovery Datasets

For the structure-recovery experiments, we use synthetic data generated by the DAG process described in Section 4.2 and Appendix B. After generation, the designated target column is removed before computing feature importance estimates. Explanations are computed independently for each feature. We construct directed edges by thresholding these magnitudes at a fixed percentile level. This procedure yields an influence graph that can be directly compared to the ground-truth DAG.

D. Additional experimental results

This section extends Section 5 with additional experimental results and analyses. Following the recommendations in (Hwang et al., 2026), our analyses address 4 perspectives regarding explanation evaluations:

Disentangling Sources of Multiplicity Evaluation. Evaluations should distinguish between variations caused by model training or selection and the stochasticity inherent in the explanation pipeline itself. We addressed this concern by fixing random seeds across all model training and selection pipelines, ensuring that any observed variability in explanations arises solely from the methods under evaluation. In addition, we include an additional analysis of zero-shot results using a different base model (MLP) to assess the robustness of ExplainerPFN across varying model architectures in Appendix D.1.

Magnitude-based metrics. ℓ_2 distance-based metrics are frequently used in the literature. We use the Pearson correlation coefficient since it is monotonically related to ℓ_2 distance when the vectors being compared have the same mean and variance, which we ensure via our post-processing correction pipeline. These results are presented in Section 5 and Appendix D.1.

Rank-based metrics. To better align with how explanations are used in practice, we also evaluate explanations using rank-based metrics. Specifically, we compute the top- k Jaccard similarity to measure agreement in the set of features identified as the most important (positively or negatively). We include these results in Appendix D.2.

Explanation evaluation as an interpretive task. Evaluating explanations as an interpretive task rather than a purely technical or descriptive one is essential to ensure that explanations align with real-world needs. We include a case study in Section 5.4 that demonstrates how ExplainerPFN compares to SHAP in a practical setting.

Table 5. Jaccard Top-K similarity between true Shapley values computed based on a RF (as the base predictor) and estimated Shapley values using ExplainerPFN (zero-shot predictions), as well as a MLP, a RF and TabPFN in different few-shot settings with varying numbers of training samples.

Method	Samples	BA	AB	AN	CC	EC	FL	GC	HE	HD	HP	TH
EPFN	0	0.641	0.102	0.588	0.326	0.298	0.114	0.118	0.580	0.559	0.282	0.272
MLP	2	0.257	0.205	0.329	0.256	0.263	0.310	0.226	0.214	0.104	0.128	0.563
	4	0.515	0.151	0.318	0.213	0.404	0.256	0.131	0.230	0.054	0.128	0.320
	6	0.631	0.142	0.294	0.319	0.316	0.239	0.208	0.272	0.225	0.179	0.372
	8	0.437	0.235	0.435	0.296	0.351	0.249	0.249	0.235	0.099	0.179	0.324
	10	0.333	0.197	0.383	0.276	0.456	0.263	0.239	0.202	0.122	0.154	0.367
RF	2	0.138	0.191	0.356	0.421	0.404	0.466	0.299	0.370	0.140	0.256	0.812
	4	0.439	0.367	0.446	0.455	0.649	0.414	0.400	0.317	0.185	0.308	0.729
	6	0.510	0.266	0.496	0.378	0.579	0.488	0.372	0.358	0.189	0.231	0.633
	8	0.595	0.314	0.562	0.400	0.579	0.437	0.384	0.329	0.176	0.231	0.680
	10	0.580	0.325	0.590	0.382	0.702	0.520	0.366	0.362	0.216	0.231	0.665
TabPFN	2	0.170	0.191	0.300	0.387	0.404	0.341	0.397	0.403	0.225	0.205	0.811
	4	0.311	0.364	0.454	0.437	0.579	0.454	0.382	0.374	0.194	0.308	0.742
	6	0.578	0.236	0.469	0.351	0.579	0.478	0.332	0.416	0.167	0.282	0.630
	8	0.614	0.306	0.508	0.373	0.614	0.459	0.393	0.440	0.212	0.256	0.770
	10	0.750	0.304	0.521	0.378	0.825	0.458	0.323	0.436	0.252	0.256	0.759

D.1. Zero-shot results with MLP as base model

Table 3 presents analogous results to Section 5.2, but using a MLP as f^b . ExplainerPFN achieves competitive performance across most datasets, with particularly strong performance on 4 datasets. Notably, on three datasets (Annealing, Heart Disease, and Hepatitis), ExplainerPFN outperforms all few-shot methods regardless of the number of training samples. However, performance varies substantially across datasets, with weaker results on datasets such as Abalone and Flags, suggesting that certain data characteristics may pose challenges for zero-shot estimation.

D.2. Rank-based evaluation

We evaluate rank-based explanation quality using the Jaccard top-K similarity metric, which measures the agreement between the sets of the top-K most important features (based on absolute feature importance values) from the estimated and reference Shapley values. Following the definition in (Hwang et al., 2026), given two rankings π_i and π_j induced by two feature importance vectors ϕ_i and ϕ_j , we define the Jaccard Top-K similarity using the top-k features, π_i^k and π_j^k , as follows:

$$\text{JaccardSimilarity}(\pi_i, \pi_j, k) = \frac{|\pi_i^k \cap \pi_j^k|}{|\pi_i^k \cup \pi_j^k|}, \quad (12)$$

Where a value of 1 indicates perfect agreement between the two sets of top-K features, while a value of 0 indicates no overlap. In our experiments, we set K to be one-third of the total number of features, i.e., $K = \max(1, \lfloor \frac{1}{3}|\phi| \rfloor)$.

Overall, the Jaccard Top-K results presented in Table 5,

using RF as the base model, and Table 6, using an MLP as the base model, align with the findings discussed in the case study analysis in Section 5.4: ExplainerPFN is able to identify key features in a zero-shot manner in several cases, but the between-feature scaling and offset limitations previously discussed become evident.

D.3. Structural Causal Model Recovery

We investigate whether ExplainerPFN can recover structural relationships among features in synthetic datasets generated from known DAGs. To do this, we compute graph edit distance (GED) to evaluate ExplainerPFN’s ability to reconstruct the true DAG structure of the underlying data-generating process over synthetic datasets.

Although ExplainerPFN is not trained to perform causal discovery, this experiment highlights the potential of zero-shot feature-importance estimation for uncovering dependencies between variables. This connection is motivated by the meta-training setup in Section 4.2, where each synthetic task is sampled from a SCM. Because ExplainerPFN learns to map feature interactions to Shapley value patterns without access to an explicit predictive model f^b , we hypothesize that its output may indirectly encode the underlying structural relationships.

To assess this, we estimate feature contributions for each feature x^j using a zero-shot attribution pass, $\Phi^j = F_{zs}(D \setminus \{x^j\}, x^j)$, followed by the post-processing step in Equation 10. We then aggregate the feature attributions of feature k as a predictor of feature j with $\phi_{\text{agg}}^j = \{E[|\phi^k|] \mid k \in M \setminus \{j\}\}$, where $E[|\phi^k|]$. This produces a weighted directed graph whose nodes represent features and edges represent

Table 6. Jaccard Top-K similarity between true Shapley values computed based on a MLP (as the base predictor) and estimated Shapley values using ExplainerPFN (zero-shot predictions), as well as a MLP, a RF and TabPFN in different few-shot settings with varying numbers of training samples.

Method	Samples	BA	AB	AN	CC	EC	FL	GC	HE	HD	HP	TH
MLP	0	0.738	0.461	0.371	0.428	0.474	0.269	0.170	0.617	0.505	0.077	0.453
	2	0.381	0.270	0.258	0.251	0.614	0.247	0.216	0.222	0.099	0.256	0.423
	4	0.318	0.225	0.304	0.294	0.526	0.242	0.232	0.206	0.212	<u>0.231</u>	0.277
	6	0.515	0.278	0.349	0.348	0.544	0.249	0.191	0.210	0.171	0.179	0.311
	8	0.709	0.340	0.343	0.337	0.526	0.239	0.223	0.210	0.095	0.205	0.307
	10	0.575	0.305	0.346	0.324	0.421	0.263	0.259	0.173	0.126	0.205	0.331
RF	2	0.175	0.239	0.433	0.606	0.404	0.341	0.337	0.337	0.122	0.179	0.612
	4	0.345	0.548	0.399	0.638	0.544	0.354	0.307	0.222	0.144	0.179	0.581
	6	0.367	0.506	0.338	0.631	0.649	0.381	0.321	0.284	0.185	0.179	0.558
	8	0.600	0.533	0.353	0.629	0.632	0.368	0.299	0.243	0.198	0.179	0.586
	10	0.602	0.537	0.365	0.570	0.719	0.380	0.258	0.267	0.212	0.154	0.587
TabPFN	2	0.194	0.239	0.424	0.570	0.263	0.353	0.337	0.329	0.108	0.179	<u>0.611</u>
	4	0.706	0.401	0.428	0.597	0.509	0.285	0.314	0.214	0.135	0.077	0.585
	6	0.731	0.407	0.412	0.602	0.719	0.398	0.300	0.292	0.207	0.077	0.563
	8	<u>0.811</u>	<u>0.478</u>	0.396	0.658	0.754	<u>0.412</u>	0.288	0.325	0.239	0.103	0.607
	10	0.920	0.497	0.397	<u>0.656</u>	0.754	0.466	0.234	0.317	<u>0.243</u>	0.179	0.610

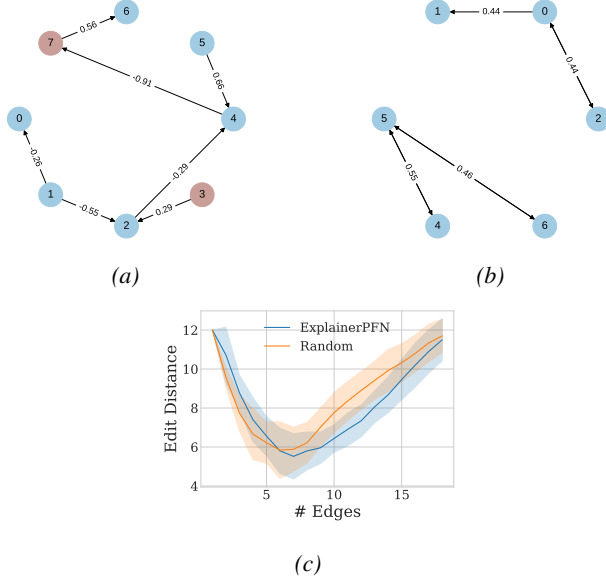


Figure 5. DAG reconstruction analyses. (a) Example of a ground truth DAG. The nodes/features marked in red are removed after generating synthetic data, but before feeding the resulting data to TabPFN. (b) Estimated DAG using ExplainerPFN with the highest-scoring 7 edges, based on feature contributions estimated by ExplainerPFN. (c) Graph Edit Distance between the true and reconstructed DAGs as a function of the number of edges kept when reconstructing the DAG using ExplainerPFN over 50 synthetic datasets generated with randomly sampled DAGs.

the strength of feature contributions.

The results shown in Figure 5 illustrate the potential of ExplainerPFN to reconstruct the underlying DAG structure of synthetic datasets. Figure 5a presents a DAG, while

Figure 5b shows its estimated reconstruction using ExplainerPFN after keeping the highest-scoring 7 edges. We observe that ExplainerPFN finds two strongly connected sets of features $\{4, 5, 6\}$ and $\{0, 1, 2\}$, but fails to connect the two sets. Figure 5c presents the graph edit distance (GED) between the true and reconstructed DAGs, as well as DAGs constructed with uniformly sampled feature importances (random), as a function of the number of edges kept when reconstructing the DAG over 50 synthetic datasets. These datasets were generated with randomly sampled DAGs, showing that ExplainerPFN is able to provide non-random DAG reconstructions, but with mild success.

E. Ablations

The analysis in this section were conducted on synthetic datasets generated using the procedure described in Section 4.2 and Appendix B. We generated datasets with varying numbers of features [2, 20] and observations [50, 10000] at step sizes of 1 and 200, respectively. For each combination of features and observations, we trained a base model and computed the corresponding SHAP explanations, which we used to evaluate ExplainerPFN’s zero-shot estimation quality over a total of 950 datasets, corresponding to combination between 19 feature sizes and 50 observation sizes. Our ablation studies highlight several insights and directions for future research.

First, the results in Figures 2 and 7 indicate that model performance is more sensitive to the number of features than to the number of observations. Although we observe substantial variability in performance across different dataset sizes (in terms of observation count), Figure 6 suggests that this

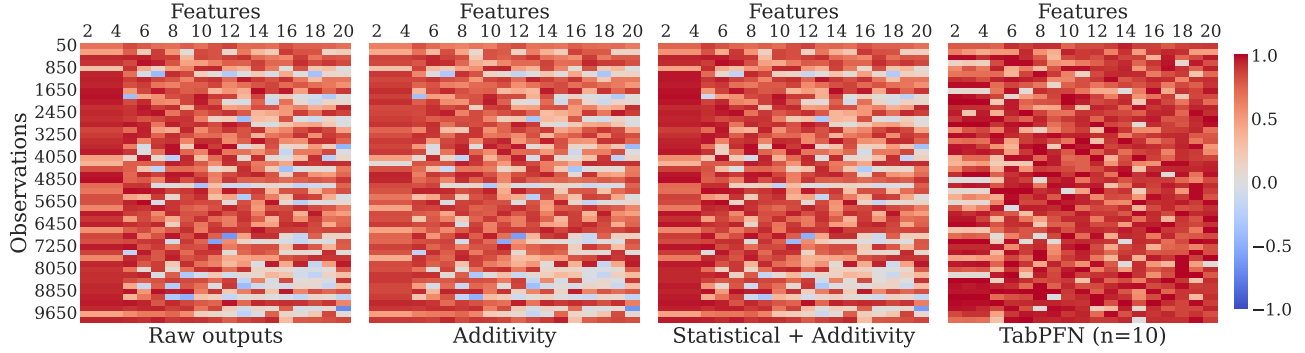


Figure 6. Pearson correlations between true and estimated Shapley values across different synthetic datasets for TabPFN with 10 training samples and ExplainerPFN outputs, including the raw outputs and correction steps.

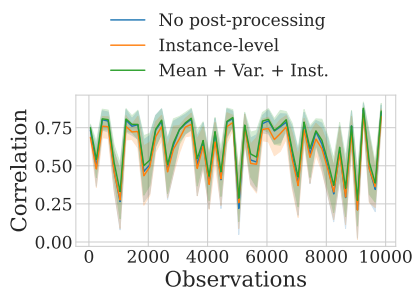


Figure 7. Pearson correlation analysis between ExplainerPFN and SHAP feature importance attribution on synthetic datasets, as a function of the number of observations using different correction steps. On average, no post-processing (blue) outperforms instance-level efficiency correction (orange), but both are consistently outperformed by applying all correction steps (green; mean-zero attributions, variance decomposition, and instance-level efficiency).

variability tends to increase as the number of observations grows. Overall, feature count appears to be the dominant factor influencing zero-shot estimation quality.

Second, ExplainerPFN achieves consistently high estimation quality on synthetic datasets, in contrast to the more variable performance observed on real-world data. This gap suggests that our synthetic data generator does not yet capture certain structural or statistical complexities present in real tabular distributions. Closing this gap represents an important area for improving future iterations of the synthetic data generation process. Nevertheless, the strong performance on synthetic datasets shows that this approach has potential to scale and effectively produce high quality explanations.

Third, we find that the different parts of the post-processing correction impact model performance in different ways. The mean-zero and variance decomposition steps are not displayed standalone since they do not affect the Pearson corre-

lation metric on their own. Instead, they improve estimation quality indirectly by aligning the scale and offset of the predicted feature attributions with the expected distribution of Shapley-based explanations, which improves the effectiveness of the additivity correction. As a result, the full correction pipeline consistently outperforms both the raw model outputs (with or without statistical normalization) and the additivity-only variant (*i.e.*, without mean-zero and variance decomposition steps), as shown in Figures 2 and 7.

Finally, Figures 2, 7, and 6 also demonstrate a degradation in performance as the number of features increases, aligning with the findings in Section 5.2. Interestingly, TabPFN trained with 10 samples exhibits the opposite trend: its performance typically improves as the number of features grows.